

Disentanglement of Sources in a Multi-Stream Variational Autoencoder

Veranika Boukun* Jörg Lücke*†

*Machine Learning Lab, Department of Medical Physics and Acoustics,
Carl von Ossietzky Universität Oldenburg, Germany

†Research Group AI, Department of Computer Science,
University of Innsbruck, Austria
veranika.boukun@uol.de, joerg.luecke@uibk.ac.at

Abstract

Variational autoencoders (VAEs) are a leading approach to address the problem of learning disentangled representations. Typically a single VAE is used and disentangled representations are sought in its continuous latent space. Here we explore a different approach by using discrete latents to combine VAE-representations of individual sources. The combination is done based on an explicit model for source combination, and we here use a linear combination model which is well suited, e.g., for acoustic data. We formally define such a multi-stream VAE (MS-VAE) approach, derive its inference and learning equations, and we numerically investigate its principled functionality. The MS-VAE is domain-agnostic, and we here explore its ability to separate sources into different streams using superimposed hand-written digits, and mixed acoustic sources in a speaker diarization task. We observe a clear separation of digits, and on speaker diarization we observe an especially low rate of missed speakers. Numerical experiments further highlight the flexibility of the approach across varying amounts of supervision and training data.

Keywords: Discrete latent variables, Disentanglement, Variational autoencoders

1 Introduction

Disentangled Representation Learning (DRL) leverages Machine Learning (ML) models to identify and separate meaningful latent variables within observed data [1]. Variational autoencoders (VAEs) are among the most popular DRL approaches. Standard VAEs promote uncorrelated, though not always fully disentangled, representations [2], and numerous extensions and modifications have been proposed, such as: applying weight coefficients to enhance disentanglement at the expense of reconstruction quality [3], using information bottleneck formulations [4], adding regularization and consistency terms [5][6]. Other VAE-based techniques impose independence constraints via total correlation [7], decompose the KL-divergence term with custom weightings [8], or use relevance indicators to identify meaningful factors of variation [9]. DLR approaches usually focus on disentanglement in continuous latent spaces. To our knowledge, JointVAE [10] is the only VAE-based DRL method that incorporates both continuous and a single discrete variation factor.

© 2025 IEEE. Personal use of this material is permitted. Permission from IEEE must be obtained for all other uses, in any current or future media, including reprinting/republishing this material for advertising or promotional purposes, creating new collective works, for resale or redistribution to servers or lists, or reuse of any copyrighted component of this work in other works.

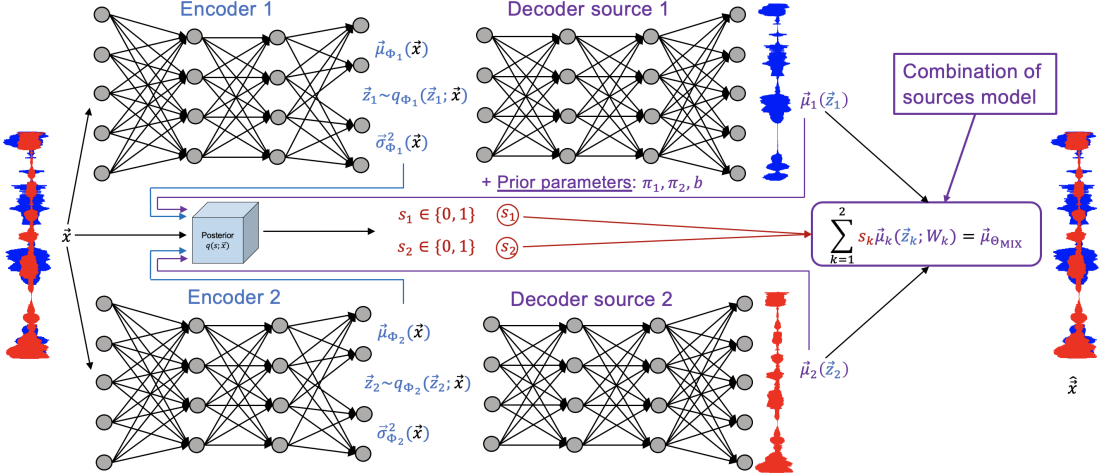


Figure 1: Schematic representation of MS-VAE for $K = 2$.

The focus of this study is the disentanglement of sources. The investigated approach makes use of a VAE-like encoding/decoding strategy. In contrast to the approaches discussed above, in this work we aim to disentangle sources using discrete latents. Furthermore, we make use of an explicit model of source combination. A linear combination is used as model, which is well-suited for many sources (including acoustic data). Variations of each source are modeled using standard VAEs with continuous latents for each source. The resulting approach is thus a hybrid of discrete and continuous latents with different roles. It will be referred to as *multi-stream VAE* (MS-VAE).

2 Proposed Method

We denote the data by $\vec{x}^{(1:N)} \in \mathbb{R}^D$, use $s_{1:K} \in \{0, 1\}^K$ for the discrete latents, and $\vec{z}_k \in \mathbb{R}^Z$ for the continuous latents (one \vec{z}_k for each source k , and we abbreviate $\vec{z}_{1:K}$ by \vec{z}). The MS-VAE decoder/generative model $p_\Theta(\vec{x})$ is then given by:

$$p_\Theta(\vec{s}) = \prod_{k=1}^K (\pi_k^{s_k} (1 - \pi_k)^{1-s_k}), \quad (1)$$

$$p_\Theta(\vec{z}) = \prod_{k=1}^K \mathcal{N}(\vec{z}_k; \vec{0}, \mathbb{I}), \quad (2)$$

$$p_\Theta(\vec{x}|\vec{s}, \vec{z}) = \text{Lap}(\vec{x}; \sum_{k=1}^K s_k \vec{\mu}(\vec{z}_k; W_k), b), \quad (3)$$

where $\vec{\mu}(\vec{z}_k; W_k)$ is the decoder DNN for source k with weights and biases given by W_k , $W_{1:K}$ are the parameters of all decoder DNNs. The set of all model parameters is thus given by $\Theta = (\vec{\pi}, W_{1:K}, b)$, where $\vec{\pi} = \pi_{1:K} \in [0, 1]^K$ are the parameters for the Bernoulli prior, and where b is the noise level of the used Laplace distribution for the observable noise. A crucial component of the MS-VAE is the explicit source combination model given in Eq. (3). Here sources are explicitly combined using \vec{s} and we will in the following use

$$\vec{\mu}_{\Theta_{\text{mix}}} = \sum_{k=1}^K s_k \vec{\mu}(\vec{z}_k; W_k) \quad (4)$$

to abbreviate the combination model.

The optimization of MS-VAE model parameters is (as for original VAEs) based on an approximate maximum likelihood approach: we seek parameters Θ^* , such that $\Theta^* = \underset{\Theta}{\text{argmax}} \mathcal{L}(\Theta) = \underset{\Theta}{\text{argmax}} \sum_n \log p_\Theta(\vec{x}^{(n)})$. Instead of directly optimizing the log-likelihood, we optimize a variational lower bound (ELBO). The ELBO

is defined by the generative model (1) to (3) and by an approximation to the exact posterior $p_\Theta(\vec{s}, \vec{z} | \vec{x})$. Here we use an approximation of the following from:

$$p_\Theta(\vec{s}, \vec{z} | \vec{x}) \approx q_\Phi(\vec{s}, \vec{z}; \vec{x}) = q(\vec{s}; \vec{z}, \vec{x}) q_\Phi(\vec{z}; \vec{x}) \quad (5)$$

The used approximate posterior generalizes the original form of ELBO [11] and leads to closed-form expressions for all D_{KL} . We assume the distributions $q_\Phi(\vec{z}; \vec{x})$ to be standard amortized variational distributions, i.e.,

$$q_\Phi(\vec{z}_k; \vec{x}) = \mathcal{N}(\vec{z}_k; \vec{\nu}(\vec{x}; \Phi_k), \text{diag}(\vec{\tau}(\vec{x}; \Phi_k))), \quad (6)$$

where we denote by $\vec{\nu}(\vec{x}; \Phi_k)$ the encoder DNN of source k for the mean. The covariance matrix $\text{diag}(\vec{\tau}(\vec{x}; \Phi_k))$ is a diagonal matrix with entries $\tau_h(\vec{x}; \Phi_k)$, and the H -dim vector $\vec{\tau}(\vec{x}; \Phi_k)$ is defined by another encoder DNN. We use Φ_k to denote all weights and biases for the encoder DNNs for source k . Based on the definitions for encoders and decoders of the MS-VAE model, its ELBO objective can canonically derived and is given by:

$$\begin{aligned} \mathcal{F}(\Phi, \Theta) = & \frac{1}{N} \left(\sum_n \int_{\vec{z}} \sum_{\vec{s}} q(\vec{s}; \vec{z}, \vec{x}^{(n)}) q_\Phi(\vec{z}; \vec{x}^{(n)}) \right. \\ & \times [\log p_\Theta(\vec{x}^{(n)} | \vec{s}, \vec{z}) + \log p_\Theta(\vec{s}) - \log q(\vec{s}; \vec{z}, \vec{x}^{(n)})] d\vec{z} \\ & \left. - \sum_n \sum_k D_{KL}[q_\Phi(\vec{z}_k; \vec{x}^{(n)}) || p_\Theta(\vec{z}_k)] \right), \end{aligned} \quad (7)$$

where D_{KL} is the Kullbach-Leibler divergence.

2.1 Computation of the Encoder Expectations

We first compute the factor $q(\vec{s}; \vec{z}, \vec{x}^{(n)})$ of the approximate posterior distribution in a numerically stable way via energies $E(\vec{x}, \vec{s}, \vec{z})$ [12]:

$$E_\Theta(\vec{x}, \vec{s}, \vec{z}) = -\log(p_\Theta(\vec{x}, \vec{s}, \vec{z})), \quad (8)$$

where $\log(p_\Theta(\vec{x}, \vec{s}, \vec{z}))$ are the log-joint probabilities. The factor $q(\vec{s}; \vec{z}, \vec{x}^{(n)})$ can then, using standard Bayes' rule and the definition (8), be computed as follows:

$$q(\vec{s}; \vec{z}, \vec{x}^{(n)}) = \frac{\exp(B^{(n)} - E_\Theta(\vec{x}^{(n)}, \vec{s}, \vec{z}))}{\sum_{\vec{s}'} \exp(B^{(n)} - E_\Theta(\vec{x}^{(n)}, \vec{s}', \vec{z}))}, \quad (9)$$

where $B^{(n)} = \min_{\vec{s}} \{E_\Theta(\vec{x}^{(n)}, \vec{s}, \vec{z})\}$ is used to ensure the exponentiation remains within the range of machine precision. The expectations of a function $f(\vec{x}, \vec{s}, \vec{z})$ w.r.t. posterior $\mathbb{E}_{q(\vec{s}; \vec{z}, \vec{x}^{(n)})}[f(\vec{x}^{(n)}, \vec{s}, \vec{z})]$ are then:

$$\begin{aligned} \mathbb{E}_{q(\vec{s}; \vec{z}, \vec{x}^{(n)})}[f(\vec{x}^{(n)}, \vec{s}, \vec{z})] &= \frac{\sum_{\vec{s}} f(\vec{x}^{(n)}, \vec{s}, \vec{z}) \exp(B^{(n)} - E_\Theta(\vec{x}^{(n)}, \vec{s}, \vec{z}))}{\sum_{\vec{s}'} \exp(B^{(n)} - E_\Theta(\vec{x}^{(n)}, \vec{s}', \vec{z}))}. \end{aligned} \quad (10)$$

2.2 Optimization of the Encoding and Decoding Models

The ELBO of MS-VAE is now optimized w.r.t. the encoder's parameters Φ and generator's parameters Θ . The generator parameters include the prior parameters $\vec{\pi}$ and the noise level b . All other parameters for

MS-VAE are weights and biases of DNNs. We optimize the DNN parameters by approximating gradient $\vec{\nabla}_\Phi \mathcal{F}(\Phi, \Theta)$ and $\vec{\nabla}_W \mathcal{F}(\Phi, \Theta)$. Concretely, we require for a given \vec{x} a number of M samples $\vec{z}_k^{(1:M)}$ for each k , i.e.,

$$\vec{z}_k^{(m)} \sim q_\Phi(\vec{z}_k; \vec{x}). \quad (11)$$

To be able to compute gradients, we do not draw directly from the Gaussian distribution but use the reparameterization trick [11]. The approximate gradient for the encoder parameters Φ is then given by:

$$\begin{aligned} \vec{\nabla}_\Phi \mathcal{F} &\approx \vec{\nabla}_\Phi \left[\sum_{n,m} \left[\log p_\Theta(\vec{x}^{(n)} | \vec{s}, \vec{z}_k^{(m)}) - \log q(\vec{s}; \vec{z}_k^{(m)}, \vec{x}^{(n)}) \right] \right. \\ &\quad \left. - \sum_n D_{KL}[q_\Phi(\vec{z}_k^{(m)}; \vec{x}^{(n)}) || p_\Theta(\vec{z}_k^{(m)})] \right] \end{aligned} \quad (12)$$

using reparameterization formulation:

$$\vec{z}_k^{(m)} = g(\vec{\epsilon}_k^{(m)}, \Phi_k, \vec{x}), \quad \vec{\epsilon}_k^{(m)} \sim \mathcal{N}(\vec{\epsilon}_k; \vec{0}, \mathbb{I}). \quad (13)$$

Similarly, for optimization of the decoding model, we use the approximate posterior $q_\Phi(\vec{s}, \vec{z}; \vec{x}^{(n)})$, then the gradient of the objective in (7) with respect to W can be approximated as:

$$\vec{\nabla}_W \mathcal{F} \approx -\frac{1}{b} \sum_{n,m} q(\vec{s}, \vec{z}^{(m)}; \vec{x}^{(n)}) \vec{\nabla}_W |\vec{x}^{(n)} - \vec{\mu}_{\Theta_{\text{mix}}}^{(n)}|.$$

Finally, using the result in (10), the update equations for the remaining model parameters are derived by setting the corresponding derivatives of the ELBO to zero (no gradients required). With sampling of \vec{z}_k , these updates are given by:

$$\begin{aligned} \pi_k &= \frac{1}{NM^2} \sum_{n,m} \mathbb{E}_{q(\vec{s}; \vec{z}^{(m)}, \vec{x}^{(n)})} [s_k] \\ b &= \frac{1}{DNM^2} \sum_{n,m} \mathbb{E}_{q(\vec{s}; \vec{z}^{(m)}, \vec{x}^{(n)})} [|\vec{x}^{(n)} - \vec{\mu}_{\Theta_{\text{mix}}}^{(n)}|]. \end{aligned} \quad (14)$$

Given a mixed signal, the encoder for source k ideally infers the same \vec{z}_k as it would without interference from other sources. In other words, the encoder must reliably extract information about its target source, regardless of how many other sources are active (see Fig. 1). If all encoders achieve this, signal reconstruction quality will be high, resulting in high ELBO values. Thus, optimizing the ELBO in Eq. (7) encourages the MS-VAE to encode distinct signal sources in separate streams. In contrast, each decoder's task is to reconstruct its source from the latent state; if a decoder is already trained to reconstruct a source, minimal further optimization is needed, even in the presence of other sources. We leverage this property of MS-VAE when pretraining decoders with available labels.

2.3 Discrete Case Prediction

To determine which source(s) are present or absent in a given $\vec{x}^{(n)}$, we can use an approximation of the $p(\vec{s} | \vec{x}^{(n)}) = \int p(\vec{s}, \vec{z} | \vec{x}^{(n)}) d\vec{z}$, where the marginalization over \vec{z} is approximated again using sampling:

$$p(\vec{s} | \vec{x}^{(n)}) \approx q(\vec{s}; \vec{x}^{(n)}) = \frac{1}{M^k} \sum_m q(\vec{s}; \vec{z}_k^{(m)}, \vec{x}^{(n)}), \quad (15)$$

with $q(\vec{s}; \vec{z}, \vec{x}^{(n)})$ as in (9). It is also possible to approximate the factors of posterior probability for individual sources $q(s_k = 1; \vec{x}^{(n)})$:

$$q(s_k = 1; \vec{x}^{(n)}) = \sum_{\vec{s}} q(\vec{s}; \vec{x}^{(n)}) \delta(s_k = 1). \quad (16)$$

3 Experiments

3.1 Neural networks and hyperparameter settings

We used DNN architectures (encoders and decoders) from [13], each comprising five feed-forward linear blocks with ReLU activations and batch normalization. Encoder layer dimensions and input size D are: $D = 784$, (700-600-500-400-300) for MNIST, and $D = 4369$, (428-320-224-160-80) for speech. The latent space has dimension $2 \times H \times K$, where 2 stands for mean and variance in (6), $H = 20$. Decoders are mirror architectures of the encoders. We used ADAM optimizer with negligible decay (0.02% per epoch) and learning rates of $lr_1 = 0.0001$ (for all pretraining and Sec. 3.4) and $lr_2 = 0.0002$ (Sec. 3.2-3.3). The number of samples $M = 100$ and batch size $B = 8$ for Sec. 3.2 and standard $M = 1$, $B = 125$ for Sec. 3.3 and 3.4 due to increasingly large dimensionality. All training and inference were performed on an NVIDIA Tesla V100 GPU.

3.2 Proof of Concept

For the initial proof of concept, we generated an artificial dataset using digits ‘0’ and ‘1’ from MNIST dataset [14]. 100% of the corresponding training subsets were used to pretrain the individual digit decoders, or ‘experts’ (10^3 epochs), whose weights were then loaded (and fixed) into the final MS-VAE model for training (10^2 epochs). Training and testing datasets ($N_{\text{train}} = 10^4$, $N_{\text{test}} = 10^3$) were generated according to the generative model with $K = 2$, $\pi_1^{\text{gen}} = 0.3$, $\pi_2^{\text{gen}} = 0.2$, $b^{\text{gen}} = 0.1$. For $K = 2$, there are $2^K = 4$ possible binary cases, examples of these are shown in Fig. 2(a). The initial parameters were $\pi_1^{\text{init}} = \pi_2^{\text{init}} = 0.5$, $b^{\text{init}} = 1$.

To assess MS-VAE performance, we evaluated prediction accuracy and parameter convergence. The model achieved a final accuracy of 99.9% with converged parameters $\pi_1^{100} \approx 0.31$, $\pi_2^{100} \approx 0.20$, and $b^{100} \approx 0.11$. We also used individual entropy analysis [15] (applicable to MS-VAE as b is learned) which confirmed convergence of the ELBO to a entropy sum ($\mathcal{F}_{\text{train}}^{100} \approx 412.0$, $\mathcal{H}_{\text{sum}}^{100} = 412.6$) and the average posterior entropy $\mathcal{H}_{q(\vec{s}; \vec{x})}^{100} \rightarrow 0$ indicating high confidence¹. The results are shown in Fig. 2(b).

3.3 Extension to multiple sources

After confirming model viability, we extended the approach to all MNIST digits. Here we used 100% or 10% of the training data to pretrain expert decoders. Decoders pretrained on 100% of the data were used as in Sec. 3.2. For the 10% scenario, decoders were loaded and fixed during initial 100 epochs, then unfixed and further finetuned for 50 epochs. We generated training and testing datasets ($N_{\text{train}} = 5 \times 10^4$, $N_{\text{test}} = 5 \times 10^3$), with $K = 10$, $\pi_k^{\text{gen}} = 1/K = 0.1$, $b^{\text{gen}} = 0.1$. The resulting number of binary cases is $2^{10} = 1024$. The parameters were initialized as in Sec. 3.2. We observed convergence of $\pi_k^{100} = \pi_k^{150} \approx 0.1$, $b^{100} = b^{150} \approx 0.11$ and $\mathcal{F}_{\text{train}}^{100} \approx \mathcal{H}_{\text{sum}}^{100} \approx 340.0$, $\mathcal{F}_{\text{train}}^{150} \approx \mathcal{H}_{\text{sum}}^{150} \approx 354.0$.

Table 1: Quantitative comparison of average source separation with population standard deviation (3 inference runs).

	Inference time, s	Classifier accuracy, %	PSNR K=2, dB	SSIM K=2	PSNR K=3, dB	SSIM K=3
MS-VAE (100%)	6.36 ± 0.59	91.23 ± 0.14	16.53 ± 0.06	0.75 ± 0.0	15.20 ± 0.12	0.68 ± 0.01
MS-VAE (10%)	5.65 ± 0.20	90.80 ± 0.28	16.58 ± 0.06	0.71 ± 0.0	15.43 ± 0.04	0.65 ± 0.0
VAE-BSS	1.94 ± 0.53	-	12.68 ± 0.05	0.43 ± 0.0	11.10 ± 0.05	0.28 ± 0.0
VAEM-BSS	2.23 ± 0.70	-	15.57 ± 0.08	0.61 ± 0.0	11.76 ± 0.04	0.44 ± 0.0

¹See [15] for more details on entropy analysis

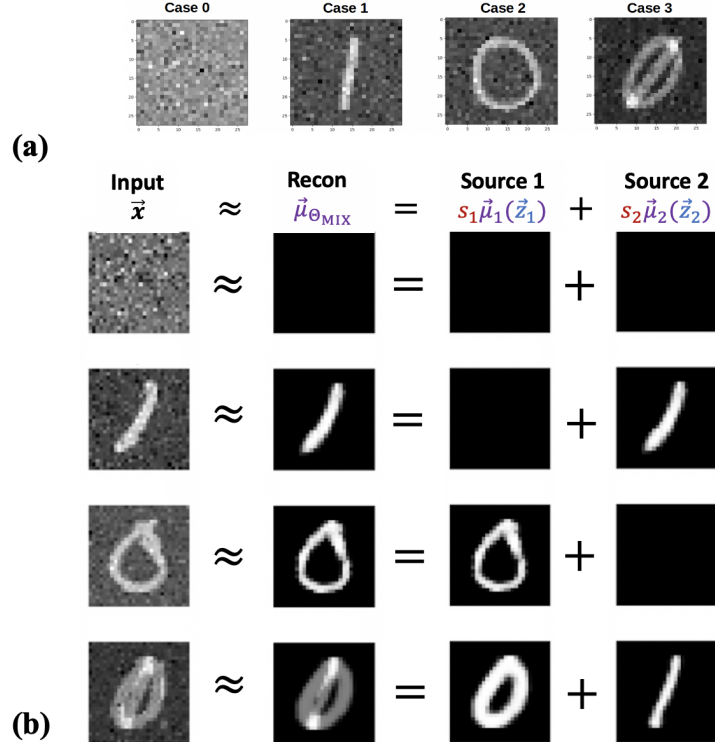


Figure 2: (a) Examples of generated artificial data points for subset of digits ‘0’ and ‘1’. (b) Schematic of source separation results.



Figure 3: Source disentanglement using the full MNIST dataset with 10% labels of available labels. Images 1 shows the input and image 2 shows the MS-VAE reconstruction; the remaining ten images correspond to the reconstructions that the MS-VAE internally uses for input reconstruction. Finetuning the model lead to slightly better reconstruction, see Tab. 1.

We also assessed standard source separation metrics by comparing to available pretrained models of [13] (with and without mask postprocessing) for $K = 2, 3$. Results in Tab. 1 were computed only on test images containing 2 or 3 overlapping sources for fair comparison. We can observe improved performance of MS-VAE in all scores. As for the disentanglement performance, mean classifier accuracy based on (15) can be viewed as a disentanglement measurement similar to the Z-min score [16]. While it is not entirely fair to compare to the unsupervised JointVAE [10], we include it here, as, to our knowledge, it is the only VAE-based disentanglement model that incorporates discrete latent factor of digit class, reporting accuracy of 88.7% on the full MNIST dataset.

3.4 Application to Acoustic Data

Speaker diarization is the semantically closest task, where each discrete latent s_k corresponds to a speaker’s activity. To test our approach, we used a 358 s recording of a conversation (2 males, 1 female) in quiet, $f_s = 48$ kHz, from a conversational behavior database [17]. Due to a mismatch in estimated statistics, we retained only 1 male, 1 female speaker, with estimated label-based statistics: $\pi_1^{\text{train}} \approx 0.30$, $\pi_1^{\text{test}} \approx 0.27$; $\pi_2^{\text{train}} \approx 0.37$, $\pi_2^{\text{test}} \approx 0.36$. The close-mic recordings were mixed and segmented into overlapping frames $T \approx 100$ ms, STFT transformed (rectangular window, 256 hop), yielding 256 frequency and 17 time bins per frame. Magnitude spectrograms were normalized to $[0, 1]$. The first 120 seconds ($N_{\text{test}} = 2812$) were used for testing; the remaining 238 seconds ($N_{\text{train}} = 5602$) for training. Individual training recordings from close-mics were processed similarly, with either 100% or 10% of data used for expert pretraining. All MS-VAE models were trained for 150 epochs with fixed decoders (unlike in Sec. 3.3).

In the close-mic recordings, the presence of speech from other participants was present. Applying a pretrained competitive Pyannote Diarization V2.1 model [18][19] to the mixture of recordings hence produced a DER of 96.73% ($K = 2$ was specified to the model). To address this issue, we replaced the inactive frames with zeros or $x_{\text{train/test}} \sim \text{Laplace}(\vec{0}, 0.0008)$ (for MS-VAE).

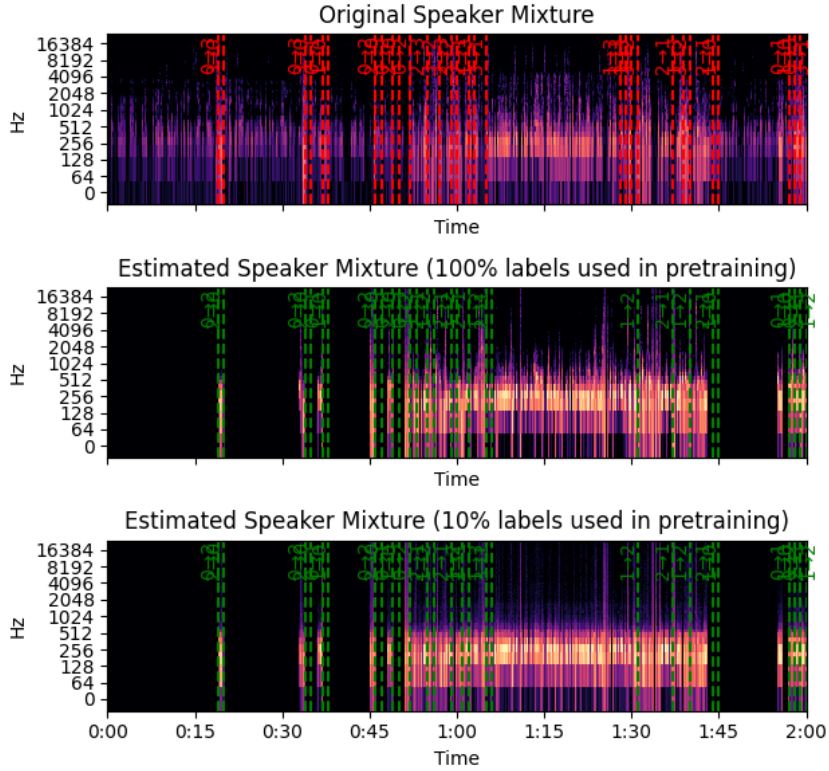


Figure 4: Spectrograms of original/estimated mixtures with decision boundaries indicating case changes, e.g., 0 \rightarrow 2: silence to speaker 1, etc., similarly to Fig. 2(a). Red: ground truth; green: predicted (Eq. (15)) averaged over 1 s intervals.

Results on the preprocessed test audio, averaged over inference 3 runs, are shown in Tab. 2. While MS-VAE models exhibit higher DER, they yield approximately 15% less missed speech (Miss.) and about 11% more precise speaker attribution (Corr.). These qualities might be especially desired in, e.g., forensics to detect and attribute the perpetrators’ speech if voice samples are available [20] as in our experimental

Table 2: Quantitative comparison in speaker diarization, with population standard deviation. MS-VAE diarization time annotations were derived from individual factors of posterior distribution Eq. (16), predictions averaged over 1 s intervals.

	Inference time, s	Average frame-wise accuracy, %	DER, %	FA, %	Miss, %	Conf, %	Corr., %
MS-VAE (100%)	13.16 ± 0.16	81.57 ± 0.11	29.90 ± 0.69	22.55 ± 0.0	2.94 ± 0.0	4.41 ± 0.0	92.65 ± 0.0
MS-VAE (10%)	12.70 ± 0.23	78.37 ± 0.03	38.24 ± 0.0	29.41 ± 0.0	4.41 ± 0.0	4.41 ± 0.0	91.18 ± 0.0
Pyannote Diarization V2.1	46.04 ± 0.50	-	18.36 ± 0.0	0.51 ± 0.0	17.54 ± 0.0	0.31 ± 0.0	82.14 ± 0.0

setup. In addition, fewer intervals were predicted by Pyannote (13 out of 16), which may contribute to lower DER. Notably, pretraining the decoder with just 10% of the data produces similar decision boundaries, as shown in Fig. 4.

4 Conclusion

In this paper, we introduced and explored the novel concept of a multi-stream VAE (MS-VAE) that incorporates source disentanglement by model design. Our approach is application-agnostic and achieving new state-of-the-art results in a specific task was not our primary goal. Nevertheless, we observed some improvements over baseline methods in disentanglement of mixed images (Tab. 1) and in speaker diarization. In disentanglement of images, examples like those in Fig. 3 demonstrate highly interpretable and clear-cut separation of individual sources (digits ‘0’, ‘8’ and ‘9’), with MS-VAE providing separate reconstructions for each digit. In speaker diarization (Tab. 2), we found the MS-VAE is particularly sensitive, missing significantly fewer frames compared to [18][19] which were trained on large corpora of speech. In contrast, the MS-VAE approach requires only a small amount of data. Some supervision is required for the MS-VAE used in this study, hence, it is not fully unsupervised like [10] or [13]. However, recent research suggests that some level of supervision may generally be necessary for effective disentanglement [21]. For real data (Sec. 3.4), it is important that training and testing sets have similar statistics for successful model learning — a requirement not shared by methods such as [18]. MS-VAE also tends to hypothesize more speech segments compared to the ground truth.

Our main goal was to addresses the largely unsolved challenge of learning disentangled representations. Our decisive novelty is the use of individual VAEs for each source, combined via discrete latents using an explicit source combination model (see Eq. 4). Future work will explore additional explicit models, such as masking [22] and occlusion [23]). While combining larger numbers of sources increases the computational complexity, up to ten sources could be readily handled with current computing resources. More sources could be managed in the future using variational approximations for the discrete latents. Recent contributions demonstrated that generative models with discrete latents can be trained very efficiently [12, 24, 22, 25], suggesting such extensions will not introduce significant computational bottlenecks. Moreover, discrete encoding may be important for achieving high-quality disentanglement representations.

5 Compliance with Ethical Standards

This is a theoretical and computational study for which no ethical approval was required. The study used conversational behavior database (not collected by the authors of this paper) for which the respective authors obtained the necessary ethical approvals (Commission for Research Impact Assessment and Ethics of the Carl von Ossietzky University of Oldenburg, approval number EK/2021/068).

6 Acknowledgments

We thank Jan Warnken for his help on derivations. This work was supported by the German Research Foundation (DFG) under grant ID 352015383 (SFB 1330, B2). We also thank the fellow researchers of the same collaborative grant (Paula Hinrichs, Volker Hohmann, Giso Grimm, project B1), who provided the conversational behavior database.

References

- [1] X. Wang et al., “Disentangled Representation Learning,” *IEEE TPAMI*, vol. 46, no. 12, pp. 9677–9696, 2024.
- [2] M. Rolinek, D. Zietlow, and G. Martius, “Variational Autoencoders Pursue PCA Directions (By Accident),” in *IEEE/CVF CVPR*, 2019, pp. 12406–12415.
- [3] I. Higgins et al., “ β -Vae: Learning Basic Visual Concepts With a Constrained Variational Framework,” in *ICLR*, 2017.
- [4] C. P. Burgess et al., “Understanding Disentangling in β -VAE,” *arXiv preprint arXiv:1804.03599*, 2018.
- [5] A. Kumar, P. Sattigeri, and A. Balakrishnan, “Variational Inference of Disentangled Latent Concepts from Unlabeled Observations,” *arXiv preprint arXiv:1711.00848*, 2017.
- [6] E. Mathieu et al., “Disentangling Disentanglement in Variational Autoencoders,” in *ICML*. PMLR, 2019, pp. 4402–4412.
- [7] H. Kim and A. Mnih, “Disentangling by Factorising,” in *ICML*. PMLR, 2018, pp. 2649–2658.
- [8] R. Chen et al., “Isolating Sources of Disentanglement in Variational Autoencoders,” *Advances in neural information processing systems*, vol. 31, 2018.
- [9] M. Kim et al., “Relevance Factor VAE: Learning and Identifying Disentangled Factors,” *arXiv preprint arXiv:1902.01568*, 2019.
- [10] E. Dupont, “Learning Disentangled Joint Continuous and Discrete Representations,” in *NeurIPS*, 2018, pp. 708–718.
- [11] D. P. Kingma and Max Welling, “Auto-Encoding Variational Bayes,” in *ICLR*, 2014.
- [12] J. Drefs, E. Guiraud, and J. Lücke, “Evolutionary Variational Optimization of Generative Models,” *JMLR*, vol. 23, no. 1, pp. 935–985, 2022.
- [13] J. Neri, R. Badeau, and P. Depalle, “Unsupervised Blind Source Separation with Variational Auto-Encoders,” in *2021 29th EUSIPCO*. IEEE, 2021, pp. 311–315.
- [14] Y. LeCun, “The MNIST Database of Handwritten Digits,” <http://yann.lecun.com/exdb/mnist/>, 1998.
- [15] S. Damm et al., “The ELBO of Variational Autoencoders Converges to a Sum of Entropies,” in *AISTATS*. PMLR, 2023, pp. 3931–3960.
- [16] M. Carbonneau et al., “Measuring Disentanglement: A Review of Metrics,” *IEEE TNNLS*, vol. 35, no. 7, pp. 8747–8761, 2022.

- [17] P. Hinrichs, V. Hohmann, and G. Grimm, “Database of Gaze, Movement and Communication Behaviour in Free Triadic Conversations,” <https://doi.org/10.5281/zenodo.17342367>, Oct. 2025.
- [18] H. Bredin et al., “pyannote.audio: Neural Building Blocks for Speaker Diarization,” in *IEEE ICASSP*, Barcelona, Spain, May 2020.
- [19] H. Bredin and A. Laurent, “End-to-end Speaker Segmentation for Overlap-aware Resegmentation,” in *Proc. Interspeech 2021*, Brno, Czech Republic, August 2021.
- [20] T. C. Nagavi et al., “Comprehensive Analysis of State-of-the-Art Approaches for Speaker Diarization,” *Automatic Speech Recognition and Translation for Low Resource Languages*, pp. 427–444, 2024.
- [21] F. Locatello et al., “A Sober Look at the Unsupervised Learning of Disentangled Representations and Their Evaluation,” *JMLR*, vol. 21, no. 209, pp. 1–62, 2020.
- [22] H. Mousavi, J. Drefs, F. Hirschberger, and J. Luecke, “Generic Unsupervised Optimization for a Latent Variable Model with Exponential Family Observables,” *JMLR*, vol. 24, no. 285, pp. 1–59, 2023.
- [23] Jörg Lücke, Richard Turner, Maneesh Sahani, and Marc Henniges, “Occlusive Components Analysis,” in *Advances in Neural Information Processing Systems*, 2009, vol. 22, pp. 1069–77.
- [24] Florian Hirschberger, Dennis Forster, and Jörg Lücke, “A Variational EM Acceleration for Efficient Clustering at Very Large Scales,” *IEEE TPAMI*, vol. 44, no. 12, pp. 9787–9801, 2022.
- [25] V. Boukun, J. Drefs, and J. Lücke, “Blind Zero-Shot Audio Restoration: A Variational Autoencoder Approach for Denoising and Inpainting,” in *Proc. Interspeech*, 2024, pp. 4823–4827.